2′-Deoxyribosyltransferase from *Bacillus psychrosaccharolyticus*: A Mesophilic-Like Biocatalyst for the Synthesis of Modified Nucleosides from a Psychrotolerant Bacterium

Alba Fresco-Taboada [1,‡], Jesús Fernández-Lucas [1,§], Carmen Acebal [1], Miguel Arroyo [1], Fernando Ramón [1], Isabel de la Mata [1,*,†] and José Miguel Mancheño [2,*,†] [iD]

[1] Department of Biochemistry and Molecular Biology I, Faculty of Biology, University Complutense of Madrid, José Antonio Nováis 12, E-28040 Madrid, Spain; albafrescotaboada@gmail.com (A.F.-T.); jesus.fernandez2@universidadeuropea.es (J.F.-L.); cacebals@ucm.es (C.A.); arroyo@bio.ucm.es (M.A.); faramon@ucm.es (F.R.)
[2] Department of Crystallography and Structural Biology, Institute Rocasolano (CSIC), Serrano 119, E-28006 Madrid, Spain
* Correspondence: idlmata@ucm.es (I.d.l.M.); xjosemi@iqfr.csic.es (J.M.M.); Tel.: +34-913-944-150 (I.d.l.M.); +34-917-459-547 (J.M.M.)
† These two researchers share the position of last author.
‡ Present address: Ingenasa, Hermanos García Noblejas 39, E-28037 Madrid, Spain.
§ Present address: Applied Biotechnology Group, European University of Madrid, Tajo s/n, Villaviciosa de Odón, E-28670 Madrid, Spain.

Abstract: Structure-function relationships of a novel 2′-deoxyribosyltransferase from the psychrotolerant bacterium *Bacillus psychrosaccharolyticus* (*Bp*NDT) have been exhaustively studied by biochemical and high resolution crystallographic analyses. Despite *Bp*NDT exhibiting some structural features characteristic of cold-adapted enzymes such as localized flexibility in critical loops, its biochemical properties are typical of mesophilic enzymes. *Bp*NDT is a highly symmetrical homohexamer with tightly associated subunits that possesses flexible and short loops bordering the active sites. The catalytic center is essentially identical to that of other mesophilic homologues. Moreover, *Bp*NDT shows that it is a mesophilic-like enzyme since it is not heat-labile and exhibits an apparent unfolding temperature (T_m) of 49 °C, being active during 96 h at 40 and 50 °C. Finally, *Bp*NDT synthesizes natural and modified nucleosides, with preference for purines as acceptors and pyrimidine nucleosides as donors. Remarkably, the synthesis of several therapeutic nucleosides has been efficiently carried out. In this sense, 5-hydroxymethyl-2′-deoxyuridine (5-HMdUrd), 7-deaza-6-hydroxypurine-2′-deoxyriboside (7-DHPdRib) and theophylline-2′-deoxyriboside were synthesized for the first time by an NDT enzyme, showing the biotechnological interest of *Bp*NDT.

Keywords: 2′-deoxyribosyltransferase; enzymatic synthesis; oligomeric assembly; protein crystallography; nucleoside analogues; therapeutic nucleosides

1. Introduction

Cold-adapted microorganisms are a valuable source of enzymes of biotechnological interest, since these biocatalysts are more efficient at low temperatures than their mesophilic and thermophilic counterparts [1,2]. Enzymes from psychrophiles present flexible structures, which render them labile at higher temperatures [3,4], but allow high turnover numbers (k_{cat}) at low-to-moderate temperatures. Psychrophiles are defined as organisms which have an optimal growth temperature at 15 °C or below,

a minimal growth temperature at 0 °C or below and a maximum growth temperature at approximately 20 °C [5]. Another group of cold-adapted microorganisms display optimal growth at about 20 °C but grow fairly well at temperatures close to 0 °C and are unable to grow at temperatures above 30 °C. These are called psychrotrophs or psychrotolerant organisms. The term psychrotolerant also encompasses mesophilic species which manage to survive at low temperatures [6]. An example of psychrotolerant bacteria is *Bacillus psychrosaccharolyticus* (CECT 4074, ATCC 23296, DSM 6), a facultative anaerobic Gram-positive bacterium that can be found in soil and lowland marshes. In the context of mesophilic *Bacillus* species, this sugar-digesting and spore-forming rod bacterium most closely resembles *Bacillus circulans*, although they differ in maximal growth temperature and in cell morphology [7]. This bacterium should be considered psychrotolerant because it reaches its optimal growth temperature at 20 °C. In fact, at low temperatures, *B. psychrosaccharolyticus* expresses cold-induced proteins, the likes of those expressed during the cold shock response in *B. subtilis*, an observation that points to systematic protein recomposition as the main psychrophilicity mechanism in this microorganism [8].

The genome of *B. psychrosaccharolyticus* has been published and a gene codifying a putative nucleoside 2′-deoxyribosyltransferase has been identified within it [9].

Nucleoside 2′-deoxyribosyltransferases (NDTs) are a group of enzymes which catalyze exchange of the 2′-deoxyribosyl moiety between 2′-deoxyribonucleosides and nucleobases. Traditionally, nucleoside synthesis has been performed by multistep chemical methods, including several protection-deprotection steps and the use of chemical reagents as well as organic solvents that are expensive and environmentally harmful [10,11]. In this sense, enzyme-catalyzed synthesis of natural and non-natural nucleosides in a one-pot, one-step reaction involving NDTs is an interesting alternative to chemical methods [12]. Nucleoside analogues are pharmacologically active compounds, which include cytotoxic, antiviral, and immunosuppressive molecules [13,14]. As an example, 5-halogenated derivatives from 2′-deoxyuridine are widely used as anticancer agents, inhibiting thymidilate synthase, an important enzyme for DNA synthesis in cell proliferation [15,16]. On the other hand, 2,6-diaminopurine nucleosides are used as drugs or prodrugs depending on their susceptibility to adenosine deaminase (ADA) activity in vivo [17].

Nucleoside 2′-deoxyribosyltransferases have been described in mesophilic microorganisms, including several lactobacilli [12,18–20] as well as in pathogen bacteria, such as *Borrelia burdogferi* [21] or protozoans like *Trypanosoma brucei* [22] or *Leishmania mexicana* [23]. In previous reports, our group described *B. psychrosaccharolyticus* as a psychrophilic source of a nucleoside 2′-deoxyribosyltransferase [24], and reported the draft genome of *B. psychrosaccharolyticus* (CECT 4074, ATCC 23296, DSM 6) under accession number AJTN02000000 [9]. A homology search with BLAST program using the amino acid sequence of the 2′-deoxyribosyltransferase from *Lactobacillus reuteri* (*Lr*NDT; NCBI reference sequence YP_001271569) allowed identification of a homologue, 142-residue sequence with 25% identity. We have previously reported the cloning and expression of this sequence and the purification of the recombinant enzyme from *B. psychrosaccharolyticus* (*Bp*NDT) [25] and showed that it is a type II nucleoside 2′-deoxyribosyltransferase, (NDT) since it catalyzes the transfer between purines and/or pyrimidines (Pur↔Pur, Pur↔Pyr, Pyr↔Pyr) (Scheme 1). This contrasts with type I nucleoside 2′-deoxyribosyltransferases (also known as purine deoxyribosyltransferases, PDTs), which are specific for purines (Pur↔Pur) [12,18,19].
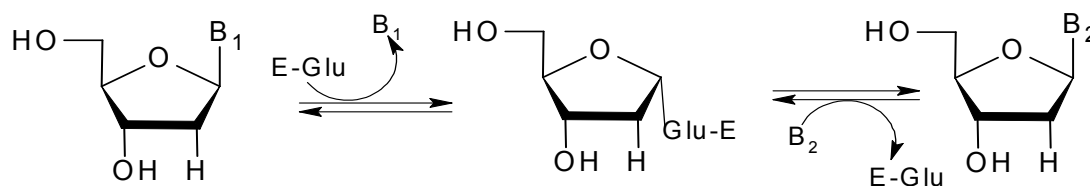
Scheme 1. 2′-deoxyribosyltransferase reaction catalyzed by *Bp*NDT. *E*, enzyme; B_1 and B_2, purine or pyrimidine.

Here, we report on biochemical and high resolution structural characterization of *Bp*NDT, including demonstration of its ability to catalyze the synthesis of several natural and non-natural nucleosides. The high resolution structure of *Bp*NDT revealed some characteristics typical of cold-adapted enzymes although its biochemical behavior is mesophilic. Finally, the enzymatic production of modified nucleosides, including antiviral and antitumoral nucleosides, was successfully carried out.

2. Results

2.1. Biochemical Characterization of Recombinant BpNDT

Optimal conditions of pH (8.0) and temperature (40 °C) were previously determined by our group [25]. Here, the effects of several cations and other additives as well as ionic strength (*I*) on *Bp*NDT activity have been studied. As shown in Table 1, neither monovalent cations nor the presence of Ba^{2+}, Ca^{2+} and Mg^{2+} significantly affected activity, whereas Co^{2+}, Cu^{2+}, Mn^{2+} and Zn^{2+} showed deleterious effects. Also, the presence of 2-mercaptoethanol did not interfere with activity as expected for an enzyme lacking cysteines like *Bp*NDT, whereas 5 mM Al^{3+} dramatically reduced enzyme activity.

Table 1. Effect of several additives on the activity of *Bp*NDT.

Additive	Relative Activity (%) at 1 mM	Relative Activity (%) at 5 mM
None	100	100
K_2SO_4	105.8	96.1
KCl	105.1	104.8
LiCl	102.0	100
Na_2SO_4	97.1	95.7
NaCl	96.6	98.2
RbCl	95.9	101.8
$BaCl_2$	98.1	91.8
$CaCl_2$	84.0	74.7
$CoCl_2$	33.0	21.8
$CuSO_4$	63.7	22.3
$MgSO_4$	86.6	95.7
$MgCl_2$	88.5	90.1
$MnCl_2$	32.6	8.1
$ZnSO_4$	91.5	57.2
$(NH4)_2SO_4$	103.8	98.8
2-mercaptoethanol	98.9	97.5
$Al_2(SO_4)_3$	90.7	18.2
$FeCl_3$	95.6	114.8
EDTA	101.3	110.8

The effect of ionic strength (*I*) on *Bp*NDT activity was studied by adding different concentrations of NaCl to reaction mixtures. Activity was unaffected at concentrations up to 1.0 M NaCl, while activity decreased 25% in the presence of 1.5 M NaCl (data not shown).

Thermal inactivation of *Bp*NDT was analyzed by pre-incubating the enzyme at different temperatures, after which aliquots were withdrawn at the indicated times and tested for activity using 2′-deoxyadenosine synthesis from 2′-deoxycitidine and adenine under standard conditions (Figure 1). Remarkably, *Bp*NDT remained stable at 40 and 50 °C for at least 96 h. Whereas at 60 and 70 °C, deoxyribosyltransferase activity diminishes following a single exponential decay, with a three-fold higher half-life at 60 °C than at 70 °C (Table 2).

Furthermore, in order to characterize the thermal stability of the enzyme, heat denaturation temperature (melting temperature), T_m, of *Bp*NDT was determined by fluorescence spectroscopy and differential scanning calorimetry (DSC) experiments (Figure 2). The effect of temperature on the intrinsic fluorescence of *Bp*NDT (excitation at 295 nm; emission from 300 to 420 nm) was evaluated at temperatures ranging from 20 to 80 °C. The values of fluorescence intensity at 335 nm were used to determine the T_m, which was 49 °C. DSC experiments showed a similar T_m value: 49.1 °C.
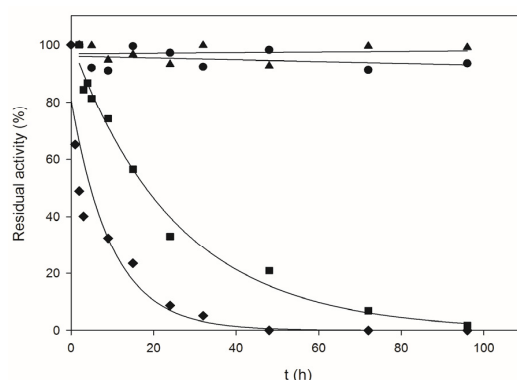

Figure 1. Thermal inactivation profile of *Bp*NDT at 40 °C (●), 50 °C (▲), 60 °C (■) and 70 °C (◆).

Table 2. Thermal inactivation parameters of *Bp*NDT.

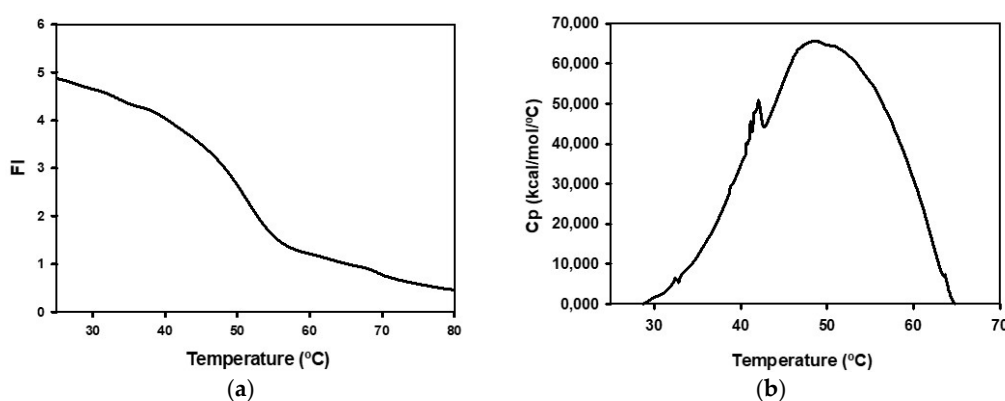| Temperature (°C)	k_d (h^{-1})	$t_{1/2}$ (h)
60	0.032	21.8
70	0.118	5.9

Figure 2. Determination of apparent melting temperature (T_m) of *Bp*NDT: (**a**) Effect of temperature on fluorescence emission at 335 nm. (**b**) Differential scanning calorimetry (DSC) analysis.

2.2. Substrate Specificity

A summary of the results obtained from the analysis of the transglycosilation reaction between natural bases and 2′-deoxynuceosides catalyzed by *Bp*NDT is shown in Table 3. According to these

results, *Bp*NDT is a type II NDT since it catalyzes the transfer of 2′-deoxyribose between pyrimidine and purine bases with a marked preference for the latter as acceptors.

2′-Deoxycytidine (dCyd) is the best donor, followed by 2′-deoxyuridine (dUrd) and thymidine (dThd). In turn, the most and least preferred acceptors are hypoxanthine (Hyp) and uracil (Ura), respectively. Compared to previously described NDTs [18,19,26,27], *Bp*NDT exhibits higher specific activities, except when compared to *Lr*NDT. The synthesis of dIno from Hyp and dAdo proceeds 5.4 times faster in the presence of *Bp*NDT than with *Lr*NDT or PDT from *Lactobacillus helveticus* (*Lh*PDT), whereas the transfer between Thd and Ura is twice faster with *Lr*NDT or *Lactococcus lactis* NDT (*Llc*NDT) than with *Bp*NDT. Formation of dAdo from Ade and Thd by *Bp*NDT is 1.5-fold and 4.3-fold more efficient than by *Lr*NDT or *Lh*PDT, respectively. Transfer between dCyd and Hyp is catalyzed by *Bp*NDT 12 times better than by NDT from *Lactobacillus fermentum* (*Lf*NDT) or *Lh*PDT.

Table 3. Analysis of the substrate specificity of *Bp*NDT in the synthesis of natural nucleosides [a].

Donor	Specific Activity (IU/mg Protein) with Acceptor				
	Ade	Ura	Cyt	Thy	Hyp
dAdo	- -	24.4	36.8	26.1	43.5
dUrd	40.0	- -	45.4	24.9	41.7
dCyd	61.2	60.0	- -	47.8	84.6
dThd	51.0	26.1	31.3	- -	38.3
dIno	20.7	15.4	18.0	40.6	- -
dGuo	38.8	16.2	36.3	8.1	22.4

[a] Reaction conditions: *Bp*NDT (0.40 µg) was incubated at 40 °C for 5 min with 10 mM substrates in 50 mM HEPES buffer, pH 8 in a final volume of 40 µL.

2.3. Structural Analysis of BpNDT

*Bp*NDT (10 mg/mL in 20 mM Tris-HCl, 0.1 M NaCl pH 8.0) crystallized in numerous conditions from the commercial screens used in the initial high throughput crystallization trials. High-quality diffraction crystals were prepared manually in 3 M sodium nitrate, 0.1 M sodium acetate trihydrate, pH 4.6 (protein/precipitant drop ratio 1:2). A complete dataset up to 1.9 Å resolution was collected at beamline ID29 at the European Synchrotron Radiation Facility (ESRF; Grenoble, France) and the crystal structure of *Bp*NDT was solved to that resolution by molecular replacement using atomic coordinates of *Lh*PDT as search model (Protein Data Bank (PDB) entry 1S2G).

*Bp*NDT crystallized as a hexamer in the trigonal *R*3 space group, with two subunits per asymmetric unit (Figure 3A) that superpose almost perfectly (r.m.s.d. for 137 Cα atoms is 0.68 Å). The final model included residues 2-138 (out of 142 amino acids) from both chains (A and B) together with 104 water molecules. The 2F_o-F_c electron density map showed continuous density for the whole protein excluding some residues coming from the same three regions in both chains: connecting loop β2-α3 (chain A: Pro42; chain B: Gln40, Leu41), connecting loop β3-α4 (chain A: Glu75; chain B: Glu75, Asn76, Tyr77) and connecting loop β4-α5 (chain A and B: Glu104). These loops appear highly flexible, which is highlighted by the high *B*-factors in these regions of the structure. All residues occupy favorable regions of the Ramachandran plot. Data collection and refinement statistics are shown in Table 4.
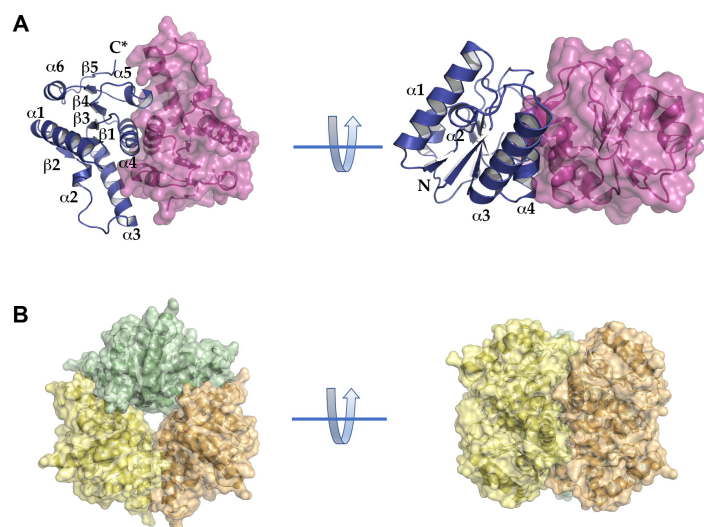
Figure 3. Overall structure of *Bp*NDT. (**A**) The two subunits of *Bp*NDT that form the asymmetric unit of the crystal are shown as ribbon model (blue) and ribbon plus transparent surface (magenta), respectively. The regular secondary structure elements are indicated. (**B**) Two orientations of the hexameric assembly identified within the *Bp*NDT crystal are shown. Each dimer is depicted in surface model.

Table 4. Data collection and refinement statistics.

	*Bp*NDT
PDB code	6EVS
Data collection	
Synchrotron source	ESRF
Beamline	ID29
Wavelength (Å)	0.9792
Space group	*R*3
Unit-cell parameters	$a = b = 107.55$, $c = 61.24$ $\alpha = \beta = 90°$, $\gamma = 120°$
Resolution range (Å)	37.07–1.90
No. of measured reflections [a]	108,568 (14,833)
No. of unique reflections	20,796 (3009)
Mean ($I/\sigma I$)	14.8 (2.9)
Completeness (%)	100 (100)
Multiplicity	5.2 (4.9)
R_{meas} (%); R_{pim} (%)	5.7 (59.8); 2.5 (26.7)
CC1/2	0.988 (0.2845)
B-factor (Wilson plot, Å^2)	32.7
Molecules/non-H atoms	
Protein	2/2257
Water	104/104
Refinement statistics	
R_{work}(%)/R_{free}(%)	17.7/21.6
Average B-factors (Å^2)	
protein	47.3
water	47.2
Rms deviation bond length (Å)	0.009
Rms deviation angles (°)	0.927
Ramachandran	
Favoured (%)	95.6
Disallowed (%)	1.48

[a] Values for the highest resolution shell are given in parentheses.

The architecture of the *Bp*NDT subunit is composed of a central, parallel, five-stranded β-sheet (with 21,345 topology), with helices packed against each of its sides (α1-α4-α5 and α3-α6, respectively). The structure is highly asymmetric due to the orientation with respect to the β-sheet and length of the α3 helix. The overall structural features of the *Bp*NDT subunit are highly similar within the 2′-deoxyribosyltransferases as can be manifested by structural similarity searches carried out either with DALI Lite server v3 [28] or FATCAT [29]. The closest structural homologue found in both cases is *Lh*PDT (r.m.s.d. of 1.5 for 130 Cα atoms and a sequence identity: 31%; PDB entry 1S2L), followed by the 2′-deoxyribosyltransferase from *Lactobacillus leichmannii* (*Ll*NDT) [30] (r.m.s.d. of 2.0 for 136 Cα atoms and a sequence identity: 26%; PDB entry: 1F8X). These two protein homologues are homohexamers endowed with D3 molecular symmetry, similarly to *Bp*NDT (see below), which resulted from the association of three dimers. In fact, the analysis of the *Bp*NDT crystal protein packing by the PISA [31] server suggested a hexamer as the highest-order stable oligomer formed by three tightly bound dimers. The contacting interface between subunits forming these dimers is large (~2740 Å^2) and comparable to those from *Lh*PDT (~3300 Å^2) or *Ll*NDT (~3200 Å^2), although much smaller than the values observed from the distant, dimeric, eukaryotic homologues from *Trypanosoma bruceii* (~4950 Å^2) or from *L. mexicana* (~4500 Å^2). This contacting interface resulted from the close packing of α4 helices from the two participating subunits and from the fact that the α5 helix of each subunit is sandwiched between helices α3# and α4# (# refers to structural elements from the other subunit). This latter

structural feature is crucial within the NDTs since it revealed that each substrate-binding pocket is in fact made up of residues contributed by the two associated subunits, supporting the idea that the dimeric assembly is the minimum catalytic unit required for 2′-deoxyribosyltransferase activity [30].

*Bp*NDT is a homohexamer with D3 molecular symmetry that results from the tight association of three dimers (Figure 3B) with a total contacting interface between them of ~7400 Å^2. The structural elements that participate in this contacting regions are the α3 and α4 helices and the corresponding α3-β3 and α4-β4 connecting loops. These elements configure a smooth, convex surface that faces the inner, three-fold molecular symmetry axis of the assembly. It is notable that the latter two connecting loops are much shorter (2 residues in both cases) than those from the opposite side of each subunit that protrude towards the bulk solvent and flank the entry to the substrate-binding pockets (loop β1-α1: 5 residues; loop α2-α3: 10 residues; loop β3-α4: 7 residues; loop β4-α5: 8 residues). As expected, whereas the structure of the contacting region with the shortest loops is highly conserved in the three hexameric enzymes *Bp*NDT, *Lh*PDT and *Ll*NDT, the region facing the solvent shows the highest structural variability, which is most probably related to the distinct substrate specificity of each particular enzyme.

Since a structural characteristic of multimeric, cold-adapted enzymes is a comparatively reduced cohesion between monomers than in the mesophilic homologues [32], we analyzed the associative behavior of *Bp*NDT in solution in order to check for the possibility of hexamer dissociation phenomena. With this aim, we studied the average molecular mass of *Bp*NDT by analytical ultracentrifugation assays. Sedimentation velocity experiments showed the existence of one homogeneous species with an experimental sedimentation coefficient of 5.9 S ($s_{20,w}$ = 6.24), which is compatible with a globular species with a molecular mass of 93 kDa. Conversely, the results from sedimentation equilibrium experiments agree well with the latter ones since they are well described by a unique species with a molecular mass of 91 kDa. Consequently, analytic ultracentrifugation experiments demonstrate that *Bp*NDT in solution is well described as a unique, homogeneous species with a molecular mass that agrees with that of a homohexamer (theoretical molecular mass of *Bp*NDT estimated from its amino acid sequence is 16,398 Da) in agreement with the crystallographic results.

2.4. Active Site of BpNDT

As an a priori cold-adapted enzyme, the crystal structure of *Bp*NDT should offer the opportunity to deduce potential structural features of the catalytic machinery of 2′-deoxyribosyltransferases reflecting adaptations to low temperature. In this sense, the superposition of its crystal structure with those from the mesophilic homologues *Ll*NDT and *Lh*PDT (Figure 4A) revealed that the catalytic residues occupy almost identical positions (Figure 4B), a characteristic that has been observed in other cases (see [32] for a review). With the aim to check the participation of such residues in the catalytic mechanism within the context of cold-adaptation, an exhaustive mutagenesis analysis was carried out by preparing a battery of single-point variants of *Bp*NDT (Table 5).

As expected, substitution of the nucleophile Glu85 abolished enzymatic activity of *Bp*NDT. This inactivating effect is obtained either by a shortening of the side chain while maintaining the carboxylate moiety (Glu85Asp variant) or by an exchange of this carboxylate for an amide group (Glu85Gln variant). These results highlight the relevance of the specific orientation and position of the nucleophile side chain in the proposed catalytic mechanism of 2′-deoxyribosyltransferases [20]. This can also be deduced from the Tyr5Phe variant where the removal of the hydroxyl group of the Tyr5 side chain fully inactivates *Bp*NDT, which reveals the critical role of the 2.9 Å H-bond between this OH group and the carboxylate OE2 atom of Glu85. On the other hand, the nearby Asp59 side chain (Asp59Asn variant) also resulted essential in the catalytic mechanism, most probably participating in the delocalization of the negative charge in the purine/pyrimidine ring during the cleavage of the glycosidic bond as proposed for *Lh*PDT [20].

Replacement of Gln40 for Glu abolishes catalytic activity of *Bp*NDT. In *Ll*NDT this residue was demonstrated to interact with the O2 and N3 atoms of the pyrimidine ring, therefore being critical

for the productive binding of pyrimidine bases [20,30]. This residue is substituted with Gly in the type II 2′-deoxyrobosyltransferases *Lh*PDT [20]. Remarkably, and in contrast to *Ll*NDT, the Gln40 side chain in *Bp*NDT is not orientated towards the substrate-binding pocket, presumably revealing that dynamic properties of the β2-α3 connecting loop should be important for catalytic activity [20,23]. In fact, Gln40 and Leu41 from chain B are ill-defined in the electron density map that together with the high *B*-factors of this loop is indicative of high flexibility. Probably, this should also be the case for the β3-α4 connecting loop of *Bp*NDT where Asp79 is located, which resulted essential for catalytic activity (Asp79Asn variant) similarly to Asp92 in *Ll*NDT or Asp95 in *Lh*PDT.
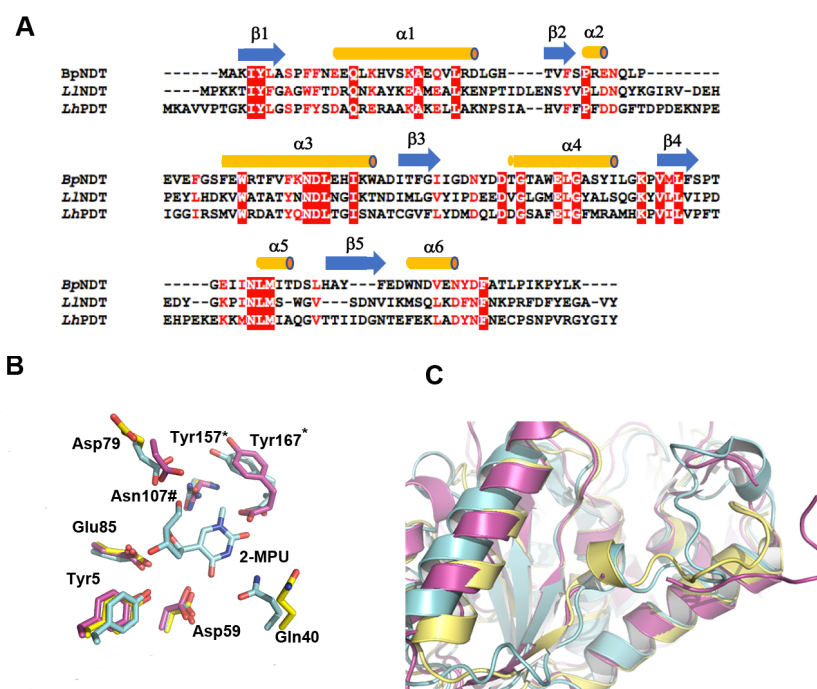

Figure 4. Structural analysis of the *Bp*NDT active site. (**A**) Multiple sequence alignment of the 2′-deoxyribosyltransferases *Bp*NDT, *Ll*NDT and *Lh*PDT. Conserved residues are depicted in white, bold characters within red boxes and highly similar ones in red characters. Catalytic important residues are marked with asterisks. (**B**) Three dimensional superposition of catalytic residues from *Bp*NDT (yellow, *sticks* model; PDB code: 6evs), *Ll*NDT (cyan, *sticks* model; PDB code: 1f8y), and *Lh*PDT (magenta, *sticks* model; PDB code: 1s2d). Numbering is with respect *Bp*NDT sequence (excluding residues marked with and asterisk). The symbol # indicates residues from the accompanying subunit. The ligand 2-methyl-pseudouridine (2-MPU) is shown to clarify the pyrimidine-binding mode (PDB code: 1f8y). (**C**) Ribbon models of *Bp*NDT, *Ll*NDT and *Lh*PDT (color code as above) highlighting the different conformation of the catalytically important loop β2-α3.

Table 5. Impact of different mutations on the activity of *Bp*NDT [a].

Mutation	None	Tyr5Phe	Tyr5His	Gln40Glu	Gln40Lys	Asp59Asn	Asp59His	Asp79Asn
Relative activity (%)	100	1.17	1.38	0	5.91	5.8	0	0
Mutation	**Asp79His**	**Glu85Asp**	**Glu85Gln**	**Glu85His**	**Asn107Asp**	**Asn107His**	**Lys142Tyr**	**ΔK142**
Relative activity (%)	0	0	0	0	0	2.12	97.72	21.5

[a] Reaction conditions: 0.40 μg of enzyme were incubated at 40 °C for 5 min with 10 mM 2′-dUrd and Ade in HEPES 50 mM buffer pH 8 in a final volume of 40 μL.

Finally, the catalytic role of the C-terminal residue of Lys142 is demonstrated in our study with the variants Lys142Tyr and ΔK142. Our results agree with previous ones showing the critical role of the carboxylate group of the C-terminal end [20,30,33]. In our case, the Lys142Tyr variant resulted as active

as native *Bp*NDT, whereas truncation of Lys142 retained significant activity (Table 5). Unfortunately, the specific location of the Lys142 side chain of *Bp*NDT could not be determined since the last four amino acids were not interpretable in the $2F_o$-F_c electron density presumably due to intrinsic disorder.

A molecular adaptation to low temperatures observed in some X-ray structures is that catalytic cavities seem to be larger and more accessible to ligands in psychrophilic enzymes than in mesophilic ones [34,35]. This can be achieved by a reduction in the length of the loops flanking the active sites, the presence of distinct conformations and/or increases in local flexibility. In this regard, superposition of the structures of *Bp*NDT, *Ll*NDT and *Lh*PDT reveals that the catalytically relevant β2-α3 connecting loop shows a conformation highly variable in the three enzymes (Figure 4C). Also, it is very much shorter in *Bp*NDT (10 residues) than in *Ll*NDT or *Lh*PDT (21 residues), which results in a more open entrance to the binding pocket. Whereas the length and conformation of the rest of the loops around the catalytic cavity (β1-α1, β3-α4 and β4-α5) are similar between *Bp*NDT and *Ll*NDT, the β4-α5 connecting region in *Lh*PDT is much longer than in *Bp*NDT (13 residues versus 7, respectively). Interestingly, these crystal structures also provide indications of dynamic regions through *B*-factor analysis. As shown in Figure 5, crystallographic *B*-factors reveal that the β2-α3, β3-α4 and β4-α5 loops of *Bp*NDT are much flexible than in *Ll*NDT or *Lh*PDT indicative of a cold-adaptation for *Bp*NDT.
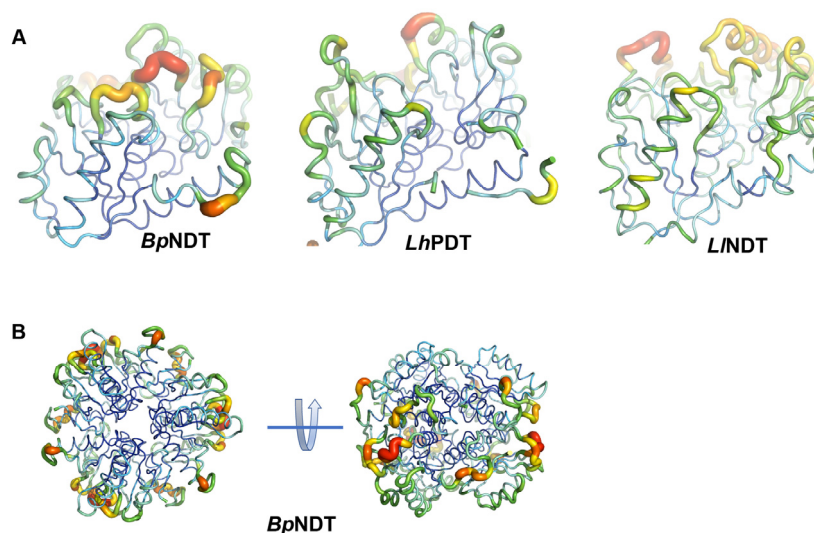

Figure 5. Analysis of flexibility regions of *Bp*NDT, *Ll*NDT and *Lh*PDT. (**A**) Crystallographic *B*-factors are used as probes to reveal flexible regions within the structures the corresponding subunits. These regions correspond to loops at the entrance to the substrate-binding site. *B*-factors are indicated by color, from blue to red, and via a putty tube representation. Red regions correspond to more flexible regions, which is clearer for *Bp*NDT. (**B**) The flexible loops of *Bp*NDT within the hexamer are located at the equatorial region of the assembly, facing the bulk solvent.

2.5. Enzymatic Production of Nucleoside Analogues

Non-natural nucleosides were synthesized from specific bases and from the best natural nucleosides, dUrd and dCyd (Table 6). *Bp*NDT was able to catalyze the transfer reaction using most of non-natural bases as acceptors, with a slight decrease in yield with respect to the one described for *Lr*NDT [18] when the donor is dUrd. As observed in the case of natural bases, higher activities were obtained when purine bases were used, such as benzimidazole, 2,6-diaminopurine and 2-fluoroadenine. Furthermore, we observed efficient catalysis of the synthesis of four nucleoside analogues: 5-hydroxymethyl-2′-deoxyuridine, 2-fluoro-2′-deoxyadenosine, 7-deaza-6-hydroxypurine-2′-deoxyriboside and theophylline-2′-deoxyriboside. This result is unprecedented for NDTs.

Table 6. *Bp*NDT-catalyzed synthesis of non-natural nucleosides from natural nucleosides and non-natural bases [a].

Acceptor	Specific Activity, IU/mg Protein (Conversion, %) with Donor:	
	dUrd	dCyd
5-Azacytosine (5-Acyt)	4.2 (42)	ND
Benzimidazole (B)	7 (75)	6.2 (68)
5-Ethyluracil (5-Eura)	3.6 (40)	3.5 (40)
2-Fluoroadenine (2-FAde)	7.5 (86)	6.2 (72)
5-(trifluoromethyl)pyrimidine-2,4(1*H*,3*H*)-dione (TFThy)	4.2 (42)	3.5 (35.5)
2,6-Diaminopurine (DAP)	8.9 (89)	7.4 (82)
6-Mercaptopurine (6-M)	5.5 (55)	4 (40)
5-Chlorouracil (5-ClUra)	3.8 (38)	3.5 (35)
5-Fluorocytosine (5-FCyt)	ND	5 (50)
5-Fluoro-2-methoxy-4(1*H*)pyrimidinone (FMP)	1.15 (18)	0.4 (5)
5-Fluorouracil (5-FUra)	4.0 (40)	4.0 (40)
5-Bromouracil (5-BrUra)	0.5 (3.6)	1.0 (3.5)
5-Iodouracil (5-IUra)	4.1 (41)	3.9 (39)
7-Deaza-6-hydroxypurine (DHP)	1.6 (15)	1.6 (16)
5-Hydroxymethyluracil (5-HMUra)	ND	4 (42)
5-Methylcytosine (5-MCyt)	0.9	0.7
Theophylline (Teo)	4.5 (45)	4.2 (42)

[a] Experimental conditions: 0.40 μg of enzyme at 40 °C for 2 h with 1.95 mM substrates in 50 mM HEPES buffer, pH 8 in a final volume of 40 μL. ND, not detected.

3. Discussion

Nowadays, psychrophilic microorganisms are being paid much attention as a source of cold-adapted enzymes with biotechnological interest, since these biocatalysts are more productive at low temperatures than their mesophilic or thermophilic counterparts [1,2]. An example of psychrotolerant bacteria is *B. psychrosaccharolyticus* (CECT 4074, ATCC 23296, DSM 6), which has been used to investigate the mechanism of solvent stress. So, Hsp33, a stress response protein that increases resistance of microorganisms in solvent stress conditions has been identified [36]. Likewise, two enzymes with biotechnological application from *B. psychrosaccharolyticus* have been described: (i) alanine racemase, which showed high catalytic activity even at 0°C and was extremely labile above 35 °C [37]; and (ii) lactate dehydrogenase, widely used in diagnostics and analytical applications [38]. Interestingly, *B. psychrosaccharolyticus* whole cells have been also reported to display nucleoside 2′-deoxyribosyltransferase activity [24] and the analysis of its genome permitted the identification of the *ndt* gene that codifies a putative NDT [9]. Subsequently, this gene was cloned and overexpressed and the recombinant protein produced and immobilized [25,39].

*Bp*NDT is the first 2′-deoxyribosyltransferase studied among psychrotolerant bacteria. Substrate specificity analyses show that it is a type II NDT since it catalyses the transfer of 2′-deoxyribose between purines and pyrimidines. Remarkably, the dependence of its catalytic activity on temperature reveals that *Bp*NDT is not heat-labile (Figure 1), a characteristic of cold-adapted enzymes that results from catalytic centres more mobile or flexible. Indeed, although we have observed that some loops flanking the substrate cavity of *Bp*NDT are more flexible than in the mesophilic *Ll*NDT or *Lh*PDT (Figures 4 and 5), it is obvious from the thermal inactivation experiments that this structural feature does not result in a heat-labile enzyme: *Bp*NDT exhibits highest activity at 40 °C and pH 8 [25]. In fact, it is active under these conditions for a longer period of time than the mesophilic *Lr*NDT: the half-time at 60 °C of *Bp*NDT (21.8 h) is remarkably higher than the one observed for *Lr*NDT (17.9 min) [18].

A consequence of mobile and flexible active sites in psychrophilic enzymes is that they have higher K_M values than their mesophilic counterparts [40]. In this case, *Bp*NDT also behaves as a mesophilic enzyme since the kinetic parameters we determined using dCyd and Ade as nucleoside donor and base acceptor, respectively (dCyd: $K_M = 2.0 \pm 0.3$ mM and k_{cat} (s^{-1}) = 24.6 ± 0.1; Ado: $K_M = 0.4 \pm 0.1$ mM and k_{cat} (s^{-1}) = 28.2 ± 0.1) compare well with published values for other mesophilic homologues [18,27,41,42].

The mesophilic character of *Bp*NDT is also observed when analysing its unfolding behaviour, either by calorimetry or by intrinsic fluorescence spectroscopy. The unfolding temperature value determined in both cases is 49 °C, an unusually high value for a psychrophilic enzyme.

Monovalent cations did not affect *Bp*NDT activity, in contrast to other reports [26]. It was only diminished by the presence of some divalent cations (Co^{2+}, Cu^{2+}, Mn^{2+}, Zn^{2+}) and Al^{3+}. That behaviour could be related to an unspecific effect since *Bp*NDT is not a metalloenzyme, and therefore these ions would create an electrostatic environment where pKa values of functional groups involved in catalysis and/or structure of the enzyme might be altered. Additionally, dramatic reduction of enzyme activity by Al^{3+} might be due to the well-known pro-oxidant activity of aluminium. On the other hand, *Bp*NDT has no cysteines in its primary sequence and 2-mercaptoethanol did not interfere with its activity. Scarcity or even absence, as in this case, of disulphide bridges is characteristic of cold-adapted enzymes [1,32].

Regarding substrate specificity, *Bp*NDT accepts different natural and non-natural bases, showing a clear preference for purines as base acceptors (Hyp > Ade > Cyt > Thy ≈ Ura) and pyrimidine nucleosides as donors (dCyd > dUrd ≈ dThd ≈ dAdo > dGuo > dIno). This substrate specificity is similar to other well-known NDTs [12,18,19] except for the strong preference for Hyp as acceptor, only comparable with that of *L. lactis subsp. lactis* NDT [26]. This result suggests that high specificity for Hyp is not exclusive for type I NDTs, traditionally associated with the metabolism of dIno for that reason, among others [19].

The enzymatic production of different nucleoside analogues was also catalyzed by *Bp*NDT, obtaining different therapeutic nucleosides, such as 5-azacytosine-2′-deoxyriboside (decitabine, an FDA approved drug for the treatment of myelodysplastic syndromes [43]), 2-fluoro-2′-deoxyadenosine (a potential prodrug for suicide gene therapy [43]), 5-fluoro-2′-deoxyuridine (floxuridine, an FDA approved drug for the treatment of advanced colon cancer, kidney cancer and stomach cancer [14]) or 5-iodo-2′-deoxyuridine (idoxuridine, approved FDA drug for the treatment of herpes simplex keratitis [14] among others). In addition, 5-hydroxymethyl-2′-deoxyuridine (5-HMdUrd), an effective prodrug that produces DNA damage in BRCA1-/- and BRCA2-/- mutant cells [44], 7-deaza-6-hydroxypurine-2′-deoxyriboside (7-DHPdRib) and theophylline-2′-deoxyriboside were synthesized for the first time by an NDT enzyme.

4. Materials and Methods

4.1. Chemicals

Culture media were purchased from Becton Dickinson (Franklin Lakes, NJ, USA). Substrates (nucleosides, 2′-deoxynucleosides and bases) and all other chemical reagents were purchased from Sigma-Aldrich (St. Louis, MO, USA).

4.2. Cloning, Sequencing and Tagging of BpNDT

The gene encoding nucleoside 2′-deoxyribosyltransferase from *B. psychrosaccharolyticus* CECT 4074 was amplified by the Polymerase Chain Reaction (PCR) with a 6-His tag coding sequence added to its 5′ end using pET28a(+)-*Bp*NDT [25] as template. DNA amplification was performed under standard conditions in a Mastercycler (Eppendorf, Hamburg, Germany) thermocycler using Pfu DNA polymerase. The amplified 0.43-kb product was inserted into a pET28a(+) vector, purified with the High Pure Plasmid Isolation Kit (Roche Diagnostics, Basel, Switzerland) and sequenced to confirm the absence of mutations. This recombinant plasmid (pET28BpndtHis) was used to transform competent *E. coli* BL21 (DE3) cells before growing them at 37 °C on LB (Luria Bertani) medium with kanamycin (50 μg/mL).

DNA manipulation and transformations were carried out according to standard methods [45]. DNA sequencing was performed by the dideoxy chain termination method [46] with an automated sequencer, 3730 DNA Analyzer (Applied Biosystems, Foster City, CA, USA).

4.3. Production and Purification of Recombinant His-Tag BpNDT

E. coli BL21 (DE3) cells harboring pET28BpndtHis were grown at 37 °C in LB medium supplemented with kanamycin (50 μg/mL). When cultures reached an optical density of 0.6 at 600 nm, expression of *BpndtHis* was induced with 0.5 mM IPTG for 2.5 h at the same temperature. Cells were then harvested by centrifugation at 3500× *g* for 10 min, resuspended in buffer A (20 mM

sodium phosphate, 500 mM NaCl, 10 mM imidazole buffer, pH 7.5) and disrupted by sonication on ice employing a Digital Sonifier 450 (Branson Ultrasonics Corporation, Danbury, CT, USA). The resulting cell extract was applied onto a 1 mL Nickel Rapid Run Cartridge (ABT, Torrejon de Ardoz, Spain) equilibrated with buffer A and washed at a flow rate of 1 mL/min until the eluate contained no protein. Adsorbed protein was then eluted using buffer B (20 mM sodium phosphate, 500 mM NaCl, 500 mM imidazole buffer at pH 7.5). Purified BpNDT-His was analyzed by SDS-PAGE using a gel containing 15% acrylamide [47]. Protein concentration was measured by the Bradford method [48].

4.4. Site Directed Mutagenesis of His-tag BpNDT

pET28a(+)BpndtHis was used as template to perform site directed mutagenesis of *His-tag BpNDT* using Quikchange II XL Site-Directed Mutagenesis Kit (Agilent Technologies, Santa Clara, CA, USA). The following 15 single-residue mutations were introduced: Y5F, Y5H, Q40E, Q40K, D59N, D59H, D79N, D79H, E85D, E85Q, E85H, N107D, N107H, K142Y and ΔK142. Resulting plasmids were sequenced to confirm the intended mutation or deletion and were used to transform *E. coli* BL21 (DE3) cells. Expression and purification of mutated proteins were carried out as described above for the native one.

4.5. N-Deoxyribosyltransferase Assay

Reaction mixtures contained 0.40 μg of electrophoretically pure enzyme, 10 mM 2′-deoxyuridine and 10 mM adenine in 50 mM HEPES buffer, pH 8.0 in a final volume of 40 μL. Reactions were conducted at 40 °C with shaking (30 r.p.m.) for 5 min and were stopped by addition of 40 μL of cold methanol and heating for 5 min at 95 °C. After centrifugation at 9000× *g* for 2 min, supernatants were half-diluted with water and analyzed by HPLC using an Agilent 1100 Series system (Agilent, Santa Clara, CA, USA) equipped with an ACE® C18-PFP column (dimensions: 250 × 46 mm; particle size: 5 μm) (Advanced Chromatography Technologies Ltd., Aberdeen, UK) at a flow rate of 0.980 mL/min. The nucleoside product was eluted into the diode array detector for quantification at 254 nm by applying two successive gradients: 100 to 90% trimethyl ammonium acetate and 0 to 10% acetonitrile in ten minutes followed by 90 to 100% trimethyl ammonium acetate and 10 to 0% acetonitrile in ten minutes. One unit of enzyme activity was defined as the amount of enzyme required to produce 1 μmol of product per minute under these conditions.

Synthesis of natural nucleosides was studied using 10 mM substrates (2′-deoxyribonucleosides and bases) while 2 mM was used for non-natural nucleosides. The buffer was 50 mM HEPES at pH 8.0 in both cases.

Retention times for reference compounds were as follows:

(a) Natural compounds: uracil (Ura): 5.41 min; 2′-deoxyuridine (dUrd): 9.16 min; adenine (Ade): 10.14 min; 2′-deoxyadenosine (dAdo): 15.50 min; hypoxanthine (Hyp): 7.34 min; 2′-deoxyinosine (dIno): 10.95 min; cytosine (Cyt): 4.14 min; 2′-deoxycytidine (dCyd): 8.22; thymine (Thy): 9.13 min; thymidine (dThd): 13.25; uric acid (UAc): 3.50 min; 2′-deoxyguanosine (dGuo): 13.25 min.

(b) Non-natural compounds: 5-fluorouracil (5-FUra): 5.94 min; 5-chlorouracil (5-ClUra): 8.71 min; 5-fluorocytosine (5-FCyt): 5.41 min; 5-bromouracil (5-BrUra): 10.28 min; 5-iodouracil (5-IUra): 13.10 min; 5-fluoro-2-methoxy-4(1*H*)pirimidinone (5-FMP): 8.47 min; 2,6-diaminopurine (2,6-DAP): 8.71 min; 6-mercaptopurine (6-M): 8.85 min; benzimidazole (B): 24.26 min; 5-azacytosine (5-azaCyt): 3.52 min; N-benzoyl adenine (N-BAde): 26.06 min; 5-ethyluracil (5-EtUra): 11.49 min; 2-fluoroadenine (2-FAde): 10.14 min; trifluorothymine (5-tFThy): 9.63 min; 7-deaza-6-hydroxypurine (7-DHP): 8.26 min; 4-hydroxy-2-mercapto-6-methylpyrimidine (4-HMMeP): 6.94 min; 6-propyl-2-thiouracil (6-PTUra): 18.13 min; 6-methyluracil (6-MeUra): 7.33 min; 5-hydroxymethyluracil (5-HMeUra): 4.71 min; 5-methylcytosine (5-MeCyt): 6.51 min; theophylline (Theo): 18.75 min; 5-fluoro-2′-deoxyuridine (5-FdUrd): 9.8 min; 5-fluoro-2′-deoxycytidine (5-FdCyd): 9.16 min; 5-chloro-2′-deoxyuridine (5-CldUrd): 13.3 min; 5-bromo-2′-deoxyuridine (5-BrdUrd): 15.7 min; 5-iodo-2′-deoxyuridine (5-IdUrd): 17.73 min; 5-fluoro-2-metoxy-4(1*H*)pirimidinone-2′-deoxyribose

(5-FMPdRib): 13.42 min; 2,6-diaminopurine-2′-deoxyribose (2,6-DAPdRib): 14.29 min; 6-mercaptopurine-2′-deoxyribose (6-MdRib): 11.96 min; benzimidazole-2′-deoxyribose (BdRib): 28.95 min; 5-aza-2′-deoxycytidine (5-azadCyd): 7.14 min; 5-ethyl-2′-deoxyuridine (5-EtdUrd): 14.82 min; 2-fluoro-2′-deoxyadenosine (2-FdAdo): 15.41 min; 5-trifluorothymidine (5-tFdThd): 11.49 min; 7-deaza-6-hydroxypurine-2′-deoxyribose (7-DHPdRib): 11.87 min; 5-hydroxymethyl-2′-deoxyuridine (5-HMedUrd): 7.42 min; 5-methyl-2′-deoxycytidine (5-MedCyd): 8.75 min; theophylline-2′-deoxyriboside (TheodRib): 22.9 min.

4.6. Thermal Inactivation Studies

Thermal inactivation kinetics were studied by incubating enzyme aliquots for different times (2 to 96 h) at several temperatures ranging from 40 to 70 °C. After thermal treatment, aliquots were put on ice for 5 minutes and the remaining activity was determined by incubating 5 µL of the treated enzyme with 10 mM 2′-deoxycytidine and 10 mM adenine and quantifying synthesis of 2′-deoxyadenosine at 40 °C in 50 mM HEPES buffer at pH 8.0.

Data were fit to single exponential decays assuming first-order, unimolecular and irreversible reactions involving only two different enzymatic states ($E_{active} \rightarrow E_{inactive}$). This is algebraically described by Equation (1):

$$A = A_0 \cdot e^{-k_{inac}t} \tag{1}$$

where A and A_0 are the residual and initial activities, respectively, for a given inactivation time (t) and k_{inac} is the first-order inactivation rate constant.

4.7. Effect of Ionic Strength and Cations on Enzyme Activity

The effect of ionic strength on 2′-deoxyribosyltransferase activity was studied by incubating 0.40 µg of enzyme with different concentrations of NaCl (0–1.5 M) in 50 mM HEPES buffer, pH 8.0 at 40 °C under standard conditions described for enzymatic assay. Similarly, synthesis of 2′-deoxyadenosine from 10 mM 2′-deoxyuridine and 10 mM adenine was evaluated in presence of different monovalent and divalent cations. Reaction mixtures contained 1 or 5 mM of the corresponding salts of monovalent (K_2SO_4, KCl, LiCl, Na_2SO_4, NaCl and RbCl) and divalent ($BaCl_2$, $CaCl_2$, $CoCl_2$, $CuSO_4$, $MgSO_4$, $MgCl_2$, $MnCl_2$ and $ZnSO_4$) cations. Additionally, the effects of $(NH_4)_2SO_4$, $Al_2(SO_4)_3$, $FeCl_3$, EDTA and 2-mercaptoethanol were also studied.

4.8. Analytical Ultracentrifugation Analysis

Sedimentation velocity and sedimentation equilibrium experiments for BpNDT were performed in 50 mM potassium phosphate buffer, pH 7.0 at $50,000\times g$ using an Optima XL-1 analytical ultracentrifuge (Beckman–Coulter Life Sciences, Indianapolis, IN, USA), equipped with absorbance optics, an An-60 Ti rotor and standard (12-mm optical path) double-sector center pieces of charcoal-filled Epon. Baseline offsets were determined at $200,000\times g$. The apparent sedimentation coefficient distribution, c(s), and sedimentation coefficient s were calculated from sedimentation velocity data using program SEDFIT 12.52 [49]. The whole-cell weight-average bM_w (buoyant molar mass) values were obtained by fitting experimental data to the equation for the radial concentration distribution of an ideal solute at sedimentation equilibrium, using program HETEROANALYSIS 1.1.44 [50]. The corresponding apparent weight-average molar masses (M_w) were determined from the buoyant masses, taking into account the partial specific volumes of the protein (0.738 mL/g) obtained from the amino acid composition using program SEDNTERP version 201220111 BETA [51].

4.9. Enzyme Crystallization and Data Collection

Crystallization of *Bp*NDT was performed at 291 K by the sitting-drop vapour diffusion method with Innovaplate SD-2 96-well plates using a Nanodrop Innovadyne robot. Each drop contained 250 nL of protein (9 mg/mL) in Tris–HCl buffer (20 mM Tris–HCl pH 8.0 containing 0.1 M NaCl) and

250 nL of reservoir solution. Drops were equilibrated against 65 μL reservoir solution. Crystals were observed in numerous conditions from all tested screens. After scaling and optimisation of preliminary crystallization conditions, high-quality diffraction crystals were prepared in 3 M sodium nitrate, 0.1 M sodium acetate trihydrate, pH 4.6 (protein/precipitant drop ratio 1:2).

For diffraction data collection, *Bp*NDT crystals were transferred to an optimized cryoprotectant solution consisting of mother liquor plus 10% (*v/v*) 2-methyl-2,4-pentanediol before being cooled to 100 K in a cold nitrogen-gas stream. Diffraction data were recorded on a Pilatus 6M pixel detector (Dectris LTD) at beamline ID29 at the European Synchrotron Radiation Facility (ESRF) (Grenoble, France). A total of 1800 images were collected with a 0.1° oscillation angle. Diffraction images were processed with *XDS* [52] and the space group examination was performed with *POINTLESS* from the Collaborative Computational Project N° 4 (CCP4) software package [53]. Crystals of *Bp*NDT belonged to the trigonal space group *R*3, with two molecules in the asymmetric unit and 41% solvent content within the unit cell. A summary of data collection statistics is provided in Table 4.

4.10. Structure Solution and Refinement

The structure of *Bp*NDT was solved by molecular replacement using *phenix. phaser* [54]. The atomic coordinates of nucleoside 2′-deoxyribosyltransferase from *Lactobacillus helveticus* were used as search model (*Lh*PDT; PDB entry 1S2G). Model rebuilding was performed manually using *COOT* [55] and refinement was carried out with *phenix.refine* [56] in PHENIX [57]. Refinement steps included *xyz* refinement, TLS (*T*ranslation, *L*ibration, *S*crew), individual atomic displacement parameters (ADPs), addition of ligands and solvent molecules. The refined structure has a final *R*-factor of 18.5% (R_{free} = 22.3%) for data up to 1.90 Å. Analysis of the interfacial surfaces was done with the PISA server [31]. Analysis of the secondary structure was done with the DSSP (*D*ictionary of *S*econdary *S*tructure of *P*roteins) server [58]. Stereochemistry validation was done with the Phenix MolProbity tool plus de wwPDB Deposition server. PyMOL [59] was used for structure visualization and figure preparation. Data collection and refinement statistics are listed in Table 1.

4.11. Spectroscopic Studies

The molar extinction coefficient of the native enzyme (ε_{nat}) was determined using an accurate method which includes both measured and calculated properties [58] and uses Equation (2):

$$\frac{A_{\text{nat}}}{A_{\text{unf}}} = \frac{\varepsilon_{\text{nat}}}{\varepsilon_{\text{unf}}} \tag{2}$$

where A_{nat} was the absorbance at 280 nm of *Bp*NDT (70 μg/mL) in 10 mM potassium phosphate buffer, pH 7.0; Aunf is that for unfolded protein (in presence of 6 M guanidine hydrochloride) and ε_{unf} is the molar extinction coefficient of the unfolded protein, which was calculated to be 30,940 $M^{-1} \cdot cm^{-1}$ from the amino acid composition of the enzyme using ProtParam program (http://web.expasy.org/protparam).

The effect of temperature on fluorescence spectra of pure *Bp*NDT was evaluated from 20 to 80 °C increasing 20 °C/h, using an excitation wavelength of 295 nm. Fluorescence emission spectra were recorded using an SLM-Aminco·Bowman Series 2 spectrofluorometer (Thermo Fisher Scientific, Waltham, MA, USA) equipped with thermostatted cell holder with 0.4 cm and 1 cm path-lengths for excitation and emission, respectively. Both excitation and emission slit widths were 5 nm. The scan rates were 60 nm/min. Protein concentration was 0.1 mg/mL in 50 mM potassium phosphate buffer, pH 7.0.

4.12. Differential Scanning Calorimetry Studies

Differential scanning calorimetry (DSC) studies were performed using a Microcalorimeter VP-DSC calorimeter (Malvern Instruments, Malvern, UK). Five scans of pure BpNDT (0.36 mg/mL in 50 mM potassium phosphate buffer, pH 7.0) were recorded from 15 to 90 °C at a scan rate of 20 °C/h.

4.13. Kinetic Studies

Kinetic parameters were calculated for the synthesis of 2′-deoxyadenosine from 2′-deoxycytidine and adenine with one substrate fixed at different concentrations (1, 2.5, 5, 7.5, 10, 15 mM) while varying the other one from 0.25 to 60 mM. K_M and k_{cat} were determined by fitting velocity data to the Michaelis–Menten model using non-linear regression analysis.

4.14. Accession Number

The atomic coordinates and structure factors have been deposited in the Protein Data Bank with the accession code 6EVS.

5. Conclusions

The present work on *Bp*NDT has provided structural and biochemical results that are apparently inconsistent regarding the adaptation of this enzyme to work at low temperatures. Hence, the thermal inactivation and unfolding experiments on *Bp*NDT showed that this enzyme is not heat labile, presenting unfolding curves typical for a mesophilic enzyme. Conversely, the structural analyses do not reveal clear-cut features characteristic of cold-adapted enzymes. In particular, the catalytic machinery of *Bp*NDT is essentially identical to that of mesophilic homologues and a great number of stabilizing interactions involved in the association of subunits within the homohexamer can be identified. In this regard, it should be remarked that most cellular adaptations to low temperatures and the underlying molecular mechanisms are not fully understood and although general trends at the molecular level are expected to exist explaining cold-adaptation, it cannot be discarded individual strategies for each protein based on specific combinations of structural alterations [32]. In the case of *Bp*NDT, we believe that features derived from its multimeric nature such as the specific topological features of this oligomer in which active sites face the solvent in an equatorial arrangement with loops at their entrances endowed with local flexibility may be critical factors underpinning its adaptation to low temperatures. Yet, we believe that our results highlight the necessity to integrate molecular information coming from functional and structural analyses of individual macromolecules into the high level cellular processes where they participate to fully explain cold-adaptation.

Finally, in this work, we have shown that one-pot, one-step nucleoside synthesis catalyzed by *Bp*NDT represents a valuable alternative to chemical methods and nucleoside phosphorylases [60]. Furthermore, *Bp*NDT is an interesting biocatalyst from an industrial point of view, since it can perform at 40 °C but also at low temperatures, minimizing undesirable chemical reactions that can occur at higher temperatures and protecting heat-labile substrates [61].

Author Contributions: I.d.l.M., J.M.M., J.F.-L. and A.F.-T. conceived and designed the experiments. All the participants contributed to the development and analysis of experimental data. I.d.l.M., J.M.M., J.F.-L., A.F.-T. and F.R. wrote the paper.

Conflicts of Interest: The authors declare no conflict of interest.

References

1. Cavicchioli, R.; Charlton, T.; Ertan, H.; Omar, S.M.; Siddiqui, K.S.; Williams, T.J. Biotechnological uses of enzymes from psychrophiles. *Microb. Biotechnol.* **2011**, *4*, 449–460. [CrossRef] [PubMed]
2. Cavicchioli, R.; Siddiqui, K.S.; Andrews, D.; Sowers, K.R. Low-temperature extremophiles and their applications. *Curr. Opin. Biotechnol.* **2002**, *13*, 253–261. [CrossRef]
3. Gerday, C.; Aittaleb, M.; Bentahir, M.; Chessa, J.P.; Claverie, P.; Collins, T.; D'Amico, S.; Dumont, J.; Garsoux, G.; Georlette, D.; et al. Cold-adapted enzymes: From fundamentals to biotechnology. *Trends Biotechnol.* **2000**, *18*, 103–107. [CrossRef]

4. D'Amico, S.; Claverie, P.; Collins, T.; Georlette, D.; Gratia, E.; Hoyoux, A.; Meuwis, M.A.; Feller, G.; Gerday, C. Molecular basis of cold adaptation. *Philos. Trans. R. Soc. Lond. Ser. B Biol. Sci.* **2002**, *357*, 917–925. [CrossRef] [PubMed]

5. Morita, R.Y. Psychrophilic bacteria. *Bacteriol. Rev.* **1975**, *39*, 144–167. [PubMed]

6. Feller, G.; Gerday, C. Psychrophilic enzymes: Molecular basis of cold adaptation. *Cell. Mol. Life Sci.* **1997**, *53*, 830–841. [CrossRef] [PubMed]

7. Larkin, J.M.; Stokes, J.L. Taxonomy of psychrophilic strains of Bacillus. *J. Bacteriol.* **1967**, *94*, 889–895. [PubMed]

8. Seo, J.B.; Kim, H.S.; Jung, G.Y.; Nam, M.H.; Chung, J.H.; Kim, J.Y.; Yoo, J.S.; Kim, C.W.; Kwon, O. Psychrophilicity of *Bacillus psychrosaccharolyticus*: A proteomic study. *Proteomics* **2004**, *4*, 3654–3659. [CrossRef] [PubMed]

9. Fresco-Taboada, A.; del Cerro, C.; Fernández-Lucas, J.; Arroyo, M.; Acebal, C.; García, J.L.; de la Mata, I. Genome of the psychrophilic bacterium *Bacillus psychrosaccharolyticus*, a potential source of 2′-deoxyribosyltransferase for industrial nucleoside synthesis. *Genome Announc.* **2013**, *1*. [CrossRef] [PubMed]

10. Lewkowicz, E.S.; Iribarren, A.M. Nucleoside phosphorylases. *Curr. Org. Chem.* **2006**, *10*, 1197–1215. [CrossRef]

11. Mikhailopulo, I.A. Biotechnology of nucleic acid constituents—State of the art and perspectives. *Curr. Org. Chem.* **2007**, *11*, 317–333. [CrossRef]

12. Fresco-Taboada, A.; de la Mata, I.; Arroyo, M.; Fernández-Lucas, J. New insights on nucleoside 2′-deoxyribosyltransferases: A versatile biocatalyst for one-pot one-step synthesis of nucleoside analogs. *Appl. Microbiol. Biotechnol.* **2013**, *97*, 3773–3785.

13. Galmarini, C.M.; Mackey, J.R.; Dumontet, C. Nucleoside analogues and nucleobases in cancer treatment. *Lancet Oncol.* **2002**, *3*, 415–424. [CrossRef]

14. Jordheim, L.P.; Durantel, D.; Zoulim, F.; Dumontet, C. Advances in the development of nucleoside and nucleotide analogues for cancer and viral diseases. *Nat. Rev. Drug Discov.* **2013**, *12*, 447–464. [CrossRef] [PubMed]

15. Brandon, M.L.; Mi, L.; Chaung, W.; Teebor, G.; Boorstein, R.J. 5-Chloro-2′-deoxyuridine cytotoxicity results from base excision repair of uracil subsequent to thymidylate synthase inhibition. *Mutat. Res.* **2000**, *459*, 161–169. [CrossRef]

16. Sato, A.; Hiramoto, A.; Uchikubo, Y.; Miyazaki, E.; Satake, A.; Naito, T.; Hiraoka, O.; Miyake, T.; Kim, H.S.; Wataya, Y. Gene expression profiles of necrosis and apoptosis induced by 5-fluoro-2′-deoxyuridine. *Genomics* **2008**, *92*, 9–17. [CrossRef] [PubMed]

17. Médici, R.; Lewkowicz, E.S.; Iribarren, A.M. Microbial synthesis of 2,6-diaminopurine nucleosides. *J. Mol. Catal. B Enzym.* **2006**, *39*, 40–44. [CrossRef]

18. Fernández-Lucas, J.; Acebal, C.; Sinisterra, J.V.; Arroyo, M.; de la Mata, I. *Lactobacillus reuteri* 2′-deoxyribosyltransferase, a novel biocatalyst for tailoring of nucleosides. *Appl. Environ. Microbiol.* **2010**, *76*, 1462–1470. [CrossRef] [PubMed]

19. Kaminski, P.A. Functional cloning, heterologous expression, and purification of two different *N*-deoxyribosyltransferases from *Lactobacillus helveticus*. *J. Biol. Chem.* **2002**, *277*, 14400–14407. [CrossRef] [PubMed]

20. Anand, R.; Kaminski, P.A.; Ealick, S.E. Structures of purine 2′-deoxyribosyltransferase, substrate complexes, and the ribosylated enzyme intermediate at 2.0 Å resolution. *Biochemistry* **2004**, *43*, 2384–2393. [CrossRef] [PubMed]

21. Lawrence, K.A.; Jewett, M.W.; Rosa, P.A.; Gherardini, F.C. *Borrelia burgdorferi* bb0426 encodes a 2′-deoxyribosyltransferase that plays a central role in purine salvage. *Mol. Microbiol.* **2009**, *72*, 1517–1529. [CrossRef] [PubMed]

22. Bosch, J.; Robien, M.A.; Mehlin, C.; Boni, E.; Riechers, A.; Buckner, F.S.; Van Voorhis, W.C.; Myler, P.J.; Worthey, E.A.; DeTitta, G.; et al. Using fragment cocktail crystallography to assist inhibitor design of *Trypanosoma brucei* nucleoside 2-deoxyribosyltransferase. *J. Med. Chem.* **2006**, *49*, 5939–5946. [CrossRef] [PubMed]

23. Crespo, N.; Sánchez-Murcia, P.A.; Gago, F.; Cejudo-Sanches, J.; Galmes, M.A.; Fernández-Lucas, J.; Mancheño, J.M. 2′-Deoxyribosyltransferase from *Leishmania mexicana*, an efficient biocatalyst for one-pot,

one-step synthesis of nucleosides from poorly soluble purine bases. *Appl. Microbiol. Biotechnol.* **2017**, *101*, 7187–7200. [CrossRef] [PubMed]

24. Fernández-Lucas, J.; Condezo, L.A.; Martínez-Lagos, F.; Sinisterra, J.V. Synthesis of 2′-deoxyribosylnucleosides using new 2′-deoxyribosyltransferase microorganism producers. *Enzym. Microb. Technol.* **2007**, *40*, 1147–1155. [CrossRef]

25. Fresco-Taboada, A.; Serra, I.; Fernandez-Lucas, J.; Acebal, C.; Arroyo, M.; Terreni, M.; de la Mata, I. Nucleoside 2′-deoxyribosyltransferase from psychrophilic bacterium *Bacillus psychrosaccharolyticus*—Preparation of an immobilized biocatalyst for the enzymatic synthesis of therapeutic nucleosides. *Molecules* **2014**, *19*, 11231–11249. [CrossRef] [PubMed]

26. Miyamoto, Y.; Masaki, T.; Chohnan, S. Characterization of *N*-deoxyribosyltransferase from *Lactococcus lactis* subsp lactis. *BBA Proteins Proteom.* **2007**, *1774*, 1323–1330. [CrossRef] [PubMed]

27. Kaminski, P.A.; Dacher, P.; Dugué, L.; Pochet, S. In vivo reshaping the catalytic site of nucleoside 2′-deoxyribosyltransferase for dideoxy- and didehydronucleosides via a single amino acid substitution. *J. Biol. Chem.* **2008**, *283*, 20053–20059. [CrossRef] [PubMed]

28. Holm, L.; Rosenström, P. Dali server: Conservation mapping in 3D. *Nucleic Acids Res.* **2010**, *38*, W545–W549. [CrossRef] [PubMed]

29. Ye, Y.; Godzik, A. Flexible structure alignment by chaining aligned fragment pairs allowing twists. *Bioinformatics* **2003**, *19*, ii246–ii255. [CrossRef] [PubMed]

30. Armstrong, S.R.; Cook, W.J.; Short, S.A.; Ealick, S.E. Crystal structures of nucleoside 2′-deoxyribosyltransferase in native and ligand-bound forms reveal architecture of the active site. *Structure* **1996**, *4*, 97–107. [CrossRef]

31. Krissinel, E.; Henrick, K. Inference of macromolecular assemblies from crystalline state. *J. Mol. Biol.* **2007**, *372*, 774–797. [CrossRef] [PubMed]

32. Feller, G.; Gerday, C. Psychrophilic enzymes: Hot topics in cold-adaptation. *Nat. Rev. Microbiol.* **2003**, *1*, 200–208. [CrossRef] [PubMed]

33. Short, S.A.; Armstrong, S.R.; Ealick, S.E.; Porter, D.J. Active site amino acids that participate in the catalytic mechanism of nucleoside 2′-deoxyribosyltransferase. *J. Biol. Chem.* **1996**, *271*, 4978–4987. [PubMed]

34. Russell, R.J.; Gerike, U.; Danson, M.J.; Hough, D.W.; Taylor, G.L. Structural adaptations of the cold-active citrate synthase from an *Antarctic bacterium*. *Structure* **1988**, *6*, 351–361. [CrossRef]

35. Aghajari, N.; Van Petegem, F.; Villeret, V.; Chessa, J.P.; Gerday, C.; Haser, R.; Van Beeumen, J. Crystal structures of a psychrophilic metalloprotease reveal new insights into catalysis by cold adapted proteases. *Proteins* **2003**, *50*, 636–647. [CrossRef] [PubMed]

36. Kang, H.; Heo, D.; Choi, S.; Kim, K.; Shim, J.; Kim, C.; Sung, H.; Yun, C. Functional characterization of Hsp33 protein from *Bacillus psychrosaccharolyticus*; additional function of HSP33 on resistance to solvent stress. *Biochem. Biophys. Res. Commun.* **2007**, *358*, 743–750. [CrossRef] [PubMed]

37. Okubo, Y.; Yokoigawa, K.; Esaki, N.; Soda, K.; Misono, H. High catalytic activity of alanine racemase from psychrophilic *Bacillus psychrosaccharolyticus* at high temperatures in the presence of pyridoxal 5′-phosphate. *FEMS Microbiol. Lett.* **2000**, *192*, 169–173. [CrossRef]

38. Nandakumar, R.; Mattiasson, B. Affinity isolation of a cold-adapted enzyme: Lactate dehydrogenase from *Bacillus psychrosaccharolyticus*. *Bioseparation* **1999**, *7*, 327–331. [CrossRef] [PubMed]

39. Fresco-Taboada, A.; Serra, I.; Arroyo, M.; Fernández-Lucas, J.; de la Mata, I.; Terreni, M. Development of an immobilized biocatalyst based on *Bacillus psychrosaccharolyticus* NDT for the preparative synthesis of trifluridine and decytabine. *Catal. Today* **2016**, *259*, 197–204. [CrossRef]

40. Xu, Y.; Feller, G.; Gerday, C.; Glansdorff, N. Metabolic enzymes from psychrophilic bacteria: Challenge of adaptation to low temperatures in ornithine carbamoyltransferase from *Moritella abyssi*. *J. Bacteriol.* **2003**, *185*, 2161–2168. [CrossRef] [PubMed]

41. Danzin, C.; Cardinaud, R. Deoxyribosyl transfer catalysis with trans-*N*-deoxyribosylase. *Eur. J. Biochem.* **1976**, *62*, 365–372. [CrossRef] [PubMed]

42. Porter, D.J.; Short, S.A. Nucleoside 2-deoxyribosyltransferase. Pre-steady-state kinetic analysis of native enzyme and mutant enzyme with an alanyl residue replacing Glu-98. *J. Biol. Chem.* **1995**, *270*, 15557–15562. [CrossRef] [PubMed]

43. Parker, W.B. Enzymology of purine and pyrimidine antimetabolites used in the treatment of cancer. *Chem. Rev.* **2009**, *109*, 2880–2893. [CrossRef] [PubMed]

44.　Clement, J.; Nakamura, J. 5-Hydroxymethyl-2′-deoxyuridine, but not temozolomide, enhances the selective synthetic lethality in BRCA1 and BRCA2- deficient cells caused by PARP inhibition. *Cancer Res.* **2013**, *73*. [CrossRef]

45.　Sambrook, J.; Fritsch, E.J.; Maniatis, T. *Molecular Cloning: A Laboratory Manual*, 2nd ed.; Cold Spring Harbor Laboratory Press: Cold Spring Harbor, NY, USA, 1989.

46.　Sanger, F.; Nicklen, S.; Coulson, A.R. DNA sequencing with chain terminating inhibitors. *Proc. Natl. Acad. Sci. USA* **1977**, *72*, 5463–5464. [CrossRef]

47.　Laemmli, U.K. Cleavage of structural proteins during the assembly of the head of bacteriophage T4. *Nature* **1970**, *227*, 680–685. [CrossRef] [PubMed]

48.　Bradford, M.M. A rapid and sensitive method for the quantitation of microgram quantities of protein utilizing the principle of protein-dye binding. *Anal. Biochem.* **1976**, *72*, 248–254. [CrossRef]

49.　Brown, P.H.; Schuck, P. Macromolecular size-and-shape distributions by sedimentation velocity analytical ultracentrifugation. *Biophys. J.* **2006**, *90*, 4651–4661. [CrossRef] [PubMed]

50.　Cole, J.L. Analysis of heterogeneous interactions. *Methods Enzymol.* **2004**, *384*, 212–232. [PubMed]

51.　Minton, A.; Jaenicke, R.; Durchschlag, H. *Alternative Strategies for the Characterization of Associations in Multicomponent Solutions via Measurement of Sedimentation Equilibrium Analytical Ultracentrifugation IV. Progress in Colloid and Polymer Science*; Springer: Berlin/Heidelberg, Germany, 1997; Volume 107, pp. 11–19.

52.　Kabsch, W. Integration, scaling, space-group assignment and post-refinement. *Acta Crystallogr. Sect. D Biol. Crystallogr.* **2010**, *66*, 133–144. [CrossRef] [PubMed]

53.　Evans, P.R. An introduction to data reduction: Space-group determination, scaling and intensity statistics. *Acta Crystallogr. Sect. D Biol. Crystallogr.* **2011**, *67*, 282–292. [CrossRef] [PubMed]

54.　McCoy, A.J. Solving structures of protein complexes by molecular replacement with Phaser. *Acta Crystallogr. Sect. D Biol. Crystallogr.* **2007**, *63*, 32–41. [CrossRef] [PubMed]

55.　Emsley, P.; Lohkamp, B.; Scott, W.G.; Cowtan, K. Features and development of Coot. *Acta Crystallogr. Sect. D Biol. Crystallogr.* **2010**, *66*, 486–501. [CrossRef] [PubMed]

56.　Afonine, P.V.; Grosse-Kunstleve, R.W.; Echols, N.; Headd, J.J.; Moriarty, N.W.; Mustyakimov, M.; Terwilliger, T.C.; Urzhumtsev, A.; Zwart, P.H.; Adams, P.D. Towards automated crystallographic structure refinement with phenix.refine. *Acta Crystallogr. Sect. D Biol. Crystallogr.* **2012**, *68*, 352–367. [CrossRef] [PubMed]

57.　Adams, P.D.; Afonine, P.V.; Bunkóczi, G.; Chen, V.B.; Davis, I.W.; Echols, N.; Headd, J.J.; Hung, L.W.; Kapral, G.J.; Grosse-Kunstleve, R.W.; et al. PHENIX: A comprehensive Python-based system for macromolecular structure solution. *Acta Crystallogr. Sect. D Biol. Crystallogr.* **2010**, *66*, 213–221. [CrossRef] [PubMed]

58.　Touw, W.G.; Baakman, C.; Black, J.; te Beek, T.A.; Krieger, E.; Joosten, R.P.; Vriend, G. A series of PDB-related databanks for everyday needs. *Nucleic Acids Res.* **2015**, *43*, D364–D368. [CrossRef] [PubMed]

59.　DeLano, W.L. *The PyMOL Molecular Graphics System*; DeLano Scientific: San Carlos, CA, USA, 2002.

60.　Bzowska, A.; Kulikowska, E.; Shugar, D. Purine nucleoside phosphorylases: Properties, functions, and clinical aspects. *Pharmacol. Ther.* **2000**, *88*, 349–425. [CrossRef]

61.　Jeon, J.; Kim, J.T.; Kang, S.; Lee, J.H.; Kim, S.J. Characterization and its potential application of two esterases derived from the Arctic sediment metagenome. *Mar. Biotechnol.* **2009**, *11*, 307–316. [CrossRef] [PubMed]